ADVANCED OPTICAL MATERIALS
www.advopticalmat.de

Influence of Outcoupling Layers on Top-Emitting Perovskite Light-Emitting Diodes

*James C. Loy, Weiming Qiu, Diane Yang, Jack Scherlag, Jonathan Scott, and Barry P. Rand**

The effects of different dielectric outcoupling layers on top-emitting perovskite light-emitting diodes (LEDs) are studied. The ability to manipulate light output via index of refraction and thickness variation of the outcoupling layer is demonstrated, leading to 27.7% improvement in external quantum efficiency (EQE) compared to devices without added outcoupling dielectric layers. Optimal dielectric thicknesses are able to be resolved for EQE enhancement across three outcoupling materials with different refractive indices. Optical simulations are shown to agree well with experimental results and allow for future optimization for various perovskite compositions with different emission spectra.

1. Introduction

Metal halide perovskite materials are promising thin-film semiconductors with applications in light-emitting diode (LED),[1–10] photovoltaic,[11–15] sensing,[16,17] and lasing technologies.[18–24] Current limitations of perovskite LEDs (PeLEDs) originate from instabilities driven by electrochemical processes, ion migration, and Joule heating.[10] Alleviating Joule heating is not straightforward in PeLEDs given the low thermally and electrically conductive halide perovskite and supporting layers.[25] More conductive transport layers have been shown to provide some assistance with heat alleviation, while other methods involve adding heat sinks external to the structure.[5,9] Heat sinks for PeLEDs would be most effective in top-emitting architectures where they can be incorporated into the substrate itself; the more commonly studied bottom-emitting PeLEDs require the use of a transparent, and generally not very thermally conductive substrate such as glass. Recently, there have been increasing efforts to develop top-emitting PeLEDs,[1,6,7,26] trading the transparent substrate for one with a much higher thermal conductivity such as silicon. Such devices have demonstrated improved efficiency roll-off due to improved thermal management.[7,26] Further, thin film perovskite laser diode development would benefit from a top-emitting PeLED architecture to realize structures that survive the high current thresholds necessary for potential electrically pumped lasing.[19] These opportunities justify further study of top-emitting PeLED architectures.

One feature the top-emitting PeLED architecture offers but which has not received focused study to-date is the use of an outcoupling layer. Anti-reflection layers are commonplace in high-performing perovskite solar cells,[14] and are analogous to outcoupling layers in top-emitting LEDs that enhance emission through the semitransparent top-electrode via modifications to the microcavity formed between metallic contacts (the cavities themselves have attracted some theoretical studies for applications in PeLEDs).[27] Here, we demonstrate that outcoupling layers can manipulate the external quantum efficiency (EQE) of top-emitting PeLEDs substantially – by 27.7%. We study the effects of our microcavity structure on device performance through a systematic analysis of three low-absorbing (extinction coefficients $k < 6 \times 10^{-4}$ at 765 nm) outcoupling layers with different refractive index and thickness; we directly manipulate only the optical character of the PeLEDs through observation of unaltered electrical response and by mapping out a full wave pattern of EQE versus outcoupling layer thickness for three dielectric materials. Furthermore, we substantiate device performance via optical simulations to validate and understand the origin of EQE enhancements.

J. C. Loy
Department of Physics
Princeton University
Princeton, NJ 08544, USA

W. Qiu
imec
Kapeldreef 75, Heverlee 3001, Belgium

D. Yang, J. Scherlag, J. Scott, B. P. Rand
Department of Electrical and Computer Engineering
Princeton University
Princeton, NJ 08544, USA
E-mail: brand@princeton.edu

B. P. Rand
Andlinger Center for Energy and the Environment
Princeton University
Princeton, NJ 08544, USA

The ORCID identification number(s) for the author(s) of this article can be found under https://doi.org/10.1002/adom.202402623

DOI: 10.1002/adom.202402623

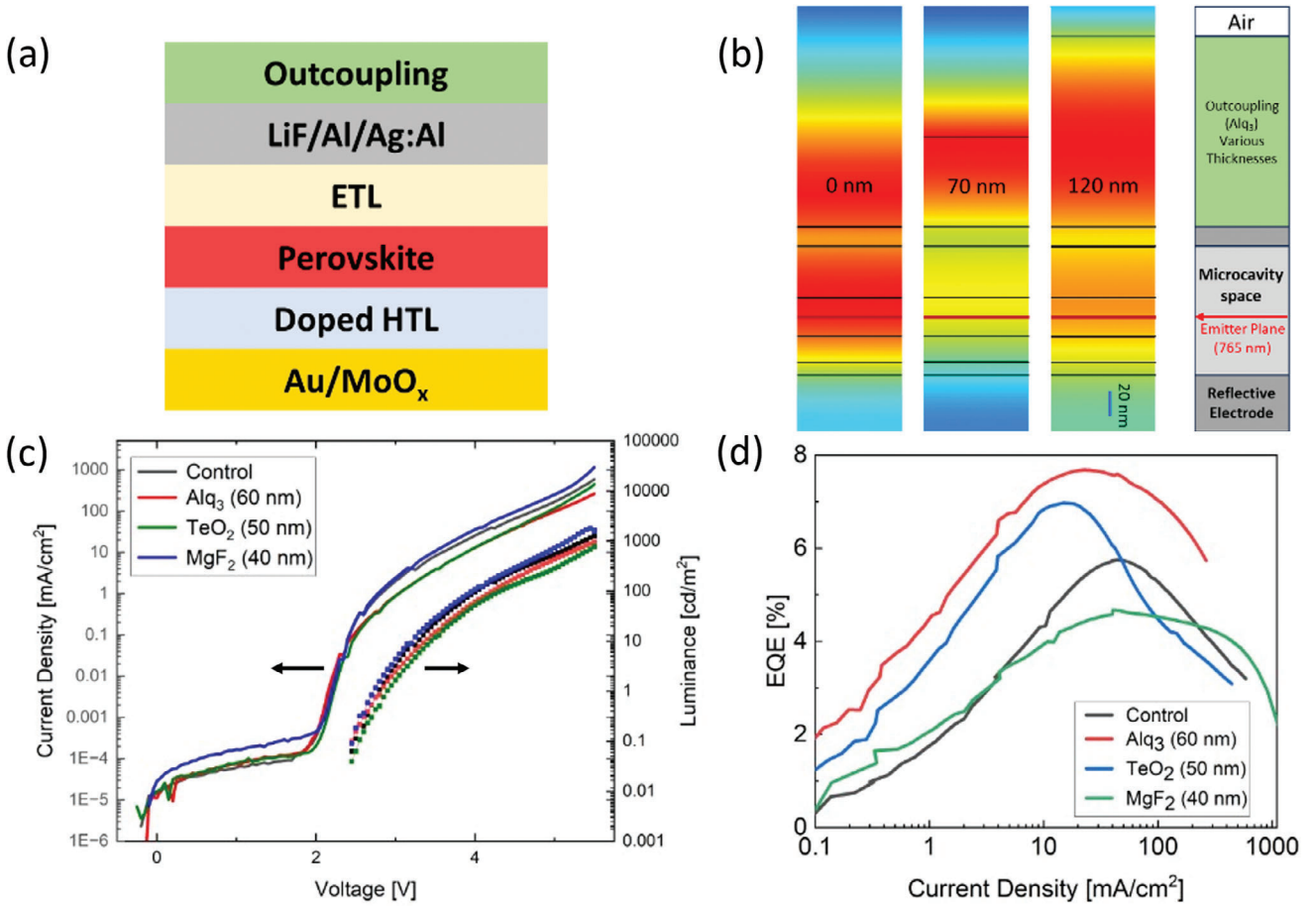

Figure 1. a) Schematic of the top-emitting PeLED architecture used in this work. b) COMSOL Multiphysics simulations of electric field amplitudes for different Alq_3 outcoupling layer thicknesses and with an emitter plane at the center of the perovskite layer, showing best coupling to far-field modes for 70 nm thickness, and increased waveguiding for devices with 0 or 120 nm thick outcoupling layers. Data are normalized to the maximum electric field strength (red), decreasing to weaker field strength (blue). c) Representative current density-luminance-voltage (*J–L–V*) characteristics for control (no outcoupling layer) devices and those with the other three dielectric outcoupling layers used in this study. d) External quantum efficiency (EQE) versus *J* for the same devices in (c).

2. Results and Discussion

We modified a well-studied near-infrared (NIR) methylammonium lead triiodide ($MAPbI_3$) PeLED (peak emission at a wavelength of ≈765 nm) into a top-emitting architecture (**Figure 1a**).[28] For a bottom reflective anode, NIR emission is compatible with numerous metals with high reflectivity such as Ag, Al, Au, or Cu, among others. In this work, we employ Au owing to the fact that other common metals react deleteriously and more readily under anodic conditions with iodide species released from the perovskite layer during operation, despite their wider window of reflectivity in the visible spectrum. Specifically, a Au/MoO_x layer serves as our anode for its superior hole injection capability compared to bare Au into the hole transport layer (HTL) composed of a mixture of poly(N,N′-bis-4-butylphenyl-N,N′-bisphenyl)benzidine (poly-TPD)[13,29,30] with poly(N-vinylcarbazole). For the top-electrode, we used an ultrathin Ag electrode with a small amount of Al to promote high transparency by interfering with the typical Volmer-Weber growth mode of ultrathin Ag, following an evaporative procedure detailed by Zhang et al.[31] We further used substrate cooling and a rapid evaporation rate to promote planar film growth. Due to the optical properties of Ag, reflectivity at the top-electrode interface has a strong influence on maximum device efficiency by directly changing the optical outcoupling efficiency of the stack; modifications to the top-electrode transparency using a dielectric outcoupling layer is a major contribution to the EQE peak as a function of outcoupling layer thickness.

When both electrodes are reflective or at least semi-reflective, as in the case studied here with two metal electrodes, the resulting microcavity gives such PeLEDs a distinct strong forward-emitting character in their angular emission profile and adds a viewing angle dependence in the emission spectrum peak. As such, the assumption of a Lambertian emission profile for microcavity devices will lead to significant errors in determining EQE. Figure S1 (Supporting Information) shows a typical electroluminescence spectrum, with a slight but clear shift in the emission peak with a viewing angle that is absent for bottom-emitting devices, while the FWHM of the spectra is narrowed by roughly 3–4 nm for the

top-emitting architecture (Figure S1, Supporting Information, inset). Figure S2 (Supporting Information) further supports the presence of a microcavity for the top-emitting PeLEDs, as the normalized intensity is strongest near the normal emission direction when compared with a typical Lambertian emission profile.

To probe the effects of outcoupling, we used three materials with a range of indices of refraction that span the range of common transparent thin film materials. Magnesium difluoride (MgF_2) is a popular anti-reflection material used in commercial applications when paired with glass owing to its index which is intermediate between that of glass and air. At the peak PeLED emission wavelength of 765 nm, the index of refraction of MgF_2 is 1.38.[15,32] Tris(8-hydroxyquinoline)aluminum(III) (Alq_3) is a widely available material commonly used in OLEDs (but rarely used as an outcoupling dielectric)[33] with an intermediate refractive index of 1.68.[34] Tellurium dioxide (TeO_2) offers high transparency and a relatively high index of 2.23 at 765 nm.[14] For outcoupling layer thicknesses on the order of the wavelength of light in that medium (a few hundred nanometers), optical interference influences the transparency and emission from the top-electrode (see Figure S3, Supporting Information). Figure 1b illustrates this effect using a simulation of the electric field for the top-emitting PeLED structure used in this work. In the control device at the left, without an outcoupling layer, there is almost equal coupling to radiative modes inside and outside of the cavity. With the addition of an outcoupling layer, waveguided modes inside the cavity appear suppressed compared to the radiative modes near the top of the outcoupling layer, indicating a promotion of far-field emission, which in turn increases the device EQE. Further outcoupling layer thickness reaches a point where the dominant emission modes become fully internal to the outcoupling layer, indicating optical outcoupling has decreased due to waveguiding in the outcoupling layer. These simulations are consistent with the peak and trough of the EQE trends for the corresponding material being modeled (Alq_3; Figure S4, Supporting Information shows similar simulations for the peak and trough thicknesses for the two other outcoupling materials).

To compare different outcoupling materials to each other, and indeed to compare different thicknesses of a single outcoupling material, the electrical character of the PeLEDs must be held constant. Figure 1c confirms comparable current density-luminance-voltage (J–L–V) behavior for typical top-emitting LEDs from each sample set with turn-on voltages of ≈2.4 V, maximum current densities exceeding 100 mA cm^{-2}, and peak luminance of ≈1000 cd m^{-2} (Figure S5, Supporting Information shows Luminance data in more detail for each outcoupling material). Figure 1d exhibits typical EQE trends for devices of each outcoupling type, with maximum EQE occurring at J between 10 and 30 mA cm^{-2}. Batch-to-batch variation influences the EQE trend of each sample between different outcoupling materials, dominated by slight differences in the top-electrode thickness resulting from the rapid rate of evaporation (see Table S1, Supporting Information for parameters of best fit for each outcoupling material run). This variation impacts the maximum EQE for each dielectric trend. However, devices within a run all have the same top-electrode thickness and variation is within acceptable limits to allow device-to-device comparison.

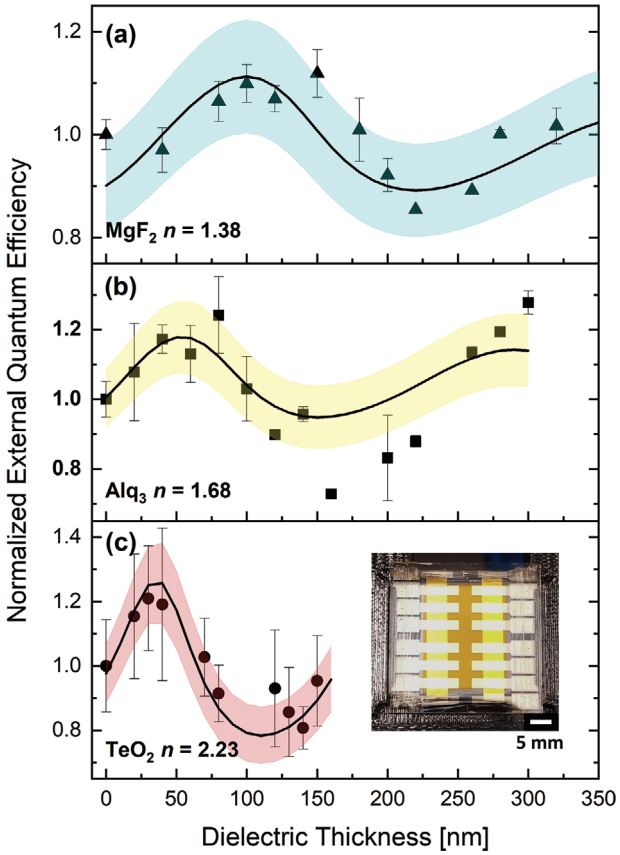

Figure 2. External quantum efficiency (EQE, normalized) versus outcoupling layer thickness for either a) MgF_2, b) Alq_3, or c) TeO_2 outcoupling layers, for nominally identical top-emitting PeLEDs. Data points correspond to experimental results, while simulations predict the solid center line in each subplot for a best fitting parameter, with the colored regions above and below indicating a 5% variation of the electrical efficiency fitting parameter. Inset: photo of a sample of 12 top-emitting pixels, defined by overlap of electrodes.

Figure 2 displays experimental EQE values normalized to the base device performance over a range of outcoupling thicknesses for each dielectric (raw EQE data for Figure 2 is plotted in Figure S6, Supporting Information). We see in all the trends a clear EQE peak at an outcoupling layer thickness at or below 100 nm, followed by the rest of the optical interference oscillation over a thickness of ≈150 nm for the highest index TeO_2 to 350 nm for the lowest index MgF_2. Notably, for all outcoupling layers, the minimum EQE exists at an outcoupling layer thickness that lies beyond zero in the second antinode of the oscillation. And, especially for the Alq_3 outcoupling layer, we see that the second peak in EQE versus outcoupling layer thickness at ≈300 nm has a nearly equivalent value as the first peak at 50–75 nm, owing to negligible absorption from the outcoupling layers of the PeLED emission. The trends are not purely sinusoidal, evident from the nonuniform period between the first half-period and second half-period of each trend, suggesting that distinct effects are contributing to the EQE adjustment. We will comment on this lack of symmetry below. For overall peak EQE, we see an improvement of 27.7% in the EQE reached for Alq_3. MgF_2 showed a more modest improvement of 11.5% over the base device, while TeO_2

yielded an enhancement of 21.1%. Figure S5 (Supporting Information) details how luminance qualitatively reflects this wave-like pattern for MgF_2.

To better understand the EQE trends, we developed a transfer-matrix method (TMM) simulation for our top-emitting PeLEDs adapted from an organic LED model detailed by Furno et al. that assumes a dipole emitter plane within the emissive layer and uses layer thicknesses and complex indices of refraction to calculate LED efficiencies and other optical behavior.[35,36] It should be noted that we are working outside one of the assumptions of the model as our perovskite medium is rather strongly self-absorbing compared to molecular emitters, due to the small Stokes shift of perovskites.[3] Despite this, we find good agreement between empirical data and the predictions of our simulator. We believe this agreement is possible due to the thin emitting layer in our LEDs, limiting the scale of reabsorption. For example, in a study of photon recycling in perovskite LEDs by Chen et al., analysis of PeLEDs with varying emitter thickness between 30 nm (which is the typical film thickness for our PeLEDs) up to 2200 nm found meaningful photon recycling contributions to performance for the thickest layers of perovskite, but concluded that for the thinnest films tested the contribution was negligible.[3] Our TMM simulations are purely optical in nature but, given that the EQE ratio relies on the internal quantum efficiency (IQE) in converting electrons to radiative recombination events inside the LED, we cannot avoid accounting for the efficiency of the electrical behavior of the LED. To this end, we utilize a unitless fitting parameter that stands in as the electrical efficiency. A closed theoretical form for this parameter is derived in Furno et al.,[35] but essentially this is the ratio of electron-hole recombination events to the density of electrical charges injected into the emitter layer. This is necessarily a parameter between 0 and 1, and while this parameter is difficult to directly measure, we can assume in a carefully controlled parallel fabrication setting that this factor is roughly constant between pixels as the electrically active layers are identical in material and thickness. This variable can be roughly extracted by comparing simulated EQE trends to our experimentally measured EQE. The shaded regions in Figure 2 are simulated EQE regions bounded by trends of constant electrical efficiency, with the solid middle lines serving as the best fit for electrical efficiency. Remarkably, all devices tend to fall within 5% of the best-fit parameter for the entire run, simultaneously affirming the predictive capabilities of the simulation and the comparability of our fabricated devices. For MgF_2 and TeO_2, an electrical efficiency of 0.5 provides the best fit, while for Alq_3 we note an electrical efficiency of 0.55 provides the best fit.

Our simulations also allow us to examine the internal cavity behavior of our microcavity devices to study precisely how the outcoupling layer is improving the EQE of the devices. Power dissipation spectra of our devices can identify how optical power is distributed, parameterized by the unit transverse wave vector u.[36] **Figure 3** calculates a top-emitting PeLED cavity with Alq_3 as the outcoupling dielectric for key thicknesses throughout the EQE oscillation we measured. We calculate Snell's law critical angle of $u = 0.439$ (25.1°), defining the escape cone for light to contribute to measured EQE as far-field radiation, and above which photons remain trapped within the device. Between $u = 0.439$ and $u = 1$ corresponds to optical power waveguided within the device itself

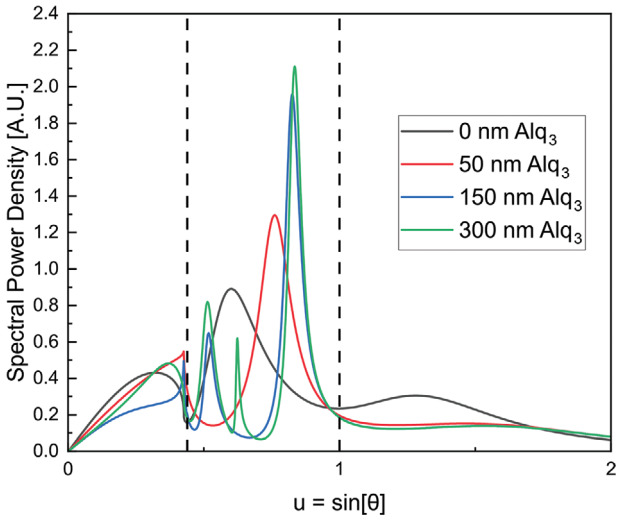

Figure 3. Simulated spectral power dissipation at 765 nm parameterized over the in-plane wavevector $u = \sin(\theta)$, where θ is the physical angle of emission. Nonphysical angles above $u = 1$ correspond to evanescent modes such as plasmon coupling. The critical angle is at $u \approx 0.439$, above which photons are waveguide trapped in the device, hence only power at $u < 0.439$ contributes to far-field emission.

as well as eventual modes trapped in the outcoupling layer as it grows thicker. Emitted power from $u > 1$ is evanescent, lacking a real out-of-plane component, and is interpreted as power coupled to plasmons in the metal electrodes surrounding the cavity, or dispersed as near-field surface waves inside the LED.[35] The control device shows a very strong peak in the evanescent coupling near $u = 1.28$, which is expected due to the two metal electrodes in close proximity to the emitter layer. As the outcoupling layer increases in thickness to the first EQE maximum near 50 nm Alq_3, we see this plasmon coupling relax to a minimum while the waveguide-trapped peak shifts to higher emission angles inside the cavity (Figure S7, Supporting Information, steps incrementally through this relaxation of the evanescent peak through addition of more outcoupling layer material). The net effect is more power emitted successfully outside the device, reflected in the plot at $u < 0.439$. Further dielectric material creates a new resonance peak inside the cavity, indicating new waveguide-trapped losses closer to the device/air interface, consistent with our simulations in Figure 1b that show a resonance develop within the outcoupling layer itself. This is a distinctly different loss profile than the plasmonic coupling that plagued the base device with no outcoupling layer, and we do not see simulation support for the return of a strong plasmonic coupling for any thicker outcoupling layer. Nearing a 300 nm thick outcoupling layer and our second EQE peak for Alq_3, we see that an extra waveguided mode develops, but the external mode is shifted to larger u where a higher density of modal states exists due to the azimuthal degree of freedom.

The good agreement between our experiments and simulations suggests that these calculations are effective for probing the large parameter space available to achieve even higher EQE device formulations. **Figure 4a** demonstrates an exploration of theoretical outcoupling materials on our top-emitting device, predicting very curious EQE trends with outcoupling refractive

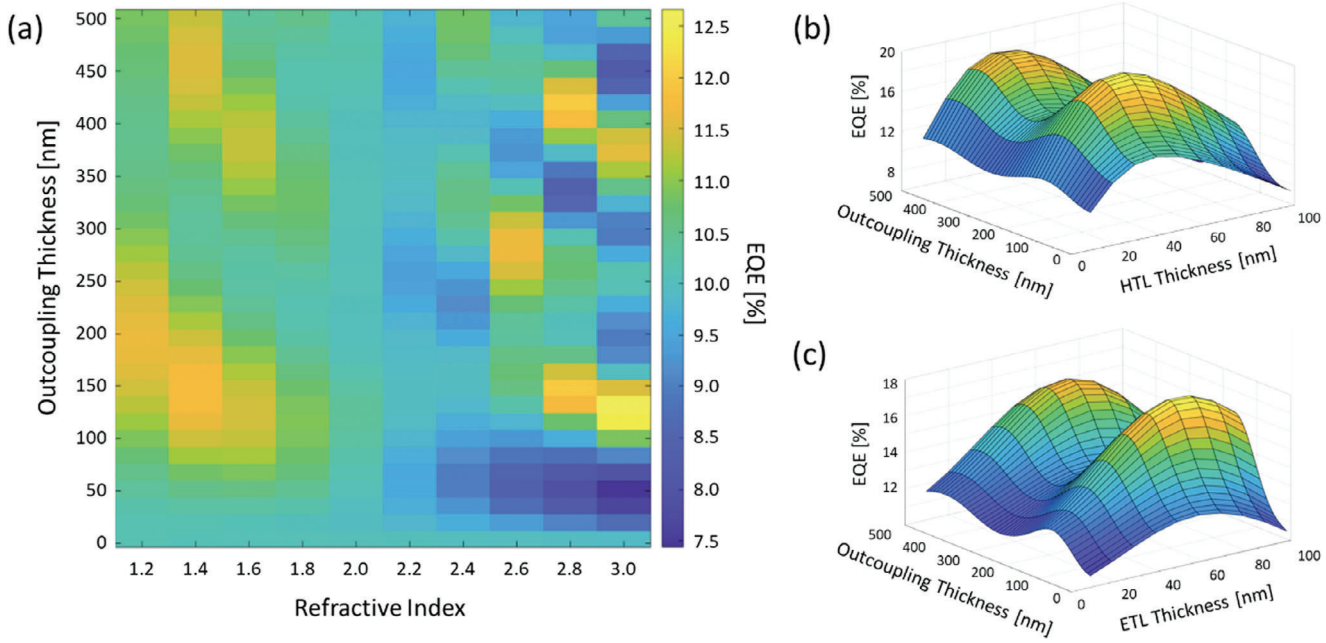

Figure 4. a) Simulated PeLED EQE for different indices of refraction and thickness (assuming no absorption and unity electrical efficiency). For each index, a different oscillation is apparent, with interesting trends predicted for materials with refractive index greater than 2.5. EQE trends for a fixed outcoupling material with varying outcoupling thickness and b) HTL or c) ETL thickness to show the EQE dependence on internal LED layers. The trends show co-dependency of outcoupling and transport layer (HTL or ETL) thickness.

index above 2.5 that further abandon uniform periodicity. This study is theoretically intriguing but is challenged by the difficulty of identifying near-zero-absorption materials at arbitrary indices of refraction. Of more practical use is using our simulation to study layers internal to the LED rather than an external outcoupling layer. The number of discrete layers necessary to produce a top-emitting architecture makes it impractical to optimize every layer iteratively, especially as the charge balance is also sensitive to the thicknesses of these layers. Figure 4b,c exhibits this by varying different charge transfer layers and showing the resulting regions of high EQE for different combinations of outcoupling and charge transport layer thickness. The dependency between all the layer thicknesses justifies the use of simulation to reduce the experimental workload. Our simulations show that our current LED architecture has strong waveguide losses that keep the overall EQE below 10% (see Figure S6, Supporting Information), but this may be circumvented by adding antireflective layers around the perovskite material or working with thinner or lower dimensional perovskite layers to reduce photon trapping.

3. Conclusion

In conclusion, we have demonstrated EQE manipulation by exploiting various dielectric outcoupling layers in a top-emitting PeLED architecture and described how the LED microcavity reacts to outcoupling through comprehensive optical modeling, including an estimate of the internal electrical efficiency. We demonstrate that outcoupling layers can improve device EQE by more than 25% for a properly chosen dielectric medium and thickness. These investigations shed light on the optical behavior of perovskite LEDs and approaches for optimization of top-emitting architectures. In particular, the lack of a thick, optically incoherent substrate in the emission path of top-emitting PeLEDs should allow them to outpace bottom-emission architectures for record efficiencies.

4. Experimental Section

Perovskite precursor solutions consisted of lead iodide (PbI_2, TCI, 99.99% purity), methylammonium iodide (MAI, Greatcell Solar Materials, >99.99% purity), and benzylammonium iodide (PMAI, Greatcell Solar Materials, >99% purity)[37] dissolved in N,N-dimethylformamide (DMF, Sigma–Aldrich, anhydrous 99.8%). All precursors were dissolved in DMF at 0.8 M, and PbI_2 required heating and stirring overnight to fully dissolve. Precursors were combined immediately preceding fabrication in a ratio of 5:5:1 PbI_2:MAI:PMAI, with DMF added to reduce the concentration to 0.2 M $MAPbI_3$. HTL precursors were prepared from poly[N,N'-bis(4-butylphenyl)-N,N'-bis(phenyl)-benzidine] (polyTPD, American Dye Source, Inc., Hole Transport Polymer ADS254BE) and poly(9-vinylcarbazole) (PVK, Sigma–Aldrich) dissolved in chlorobenzene (CB, Sigma–Aldrich, anhydrous 99.8%). A solution of 6 mg mL^{-1} polymer HTL comprised 5.62 mg mL^{-1} polyTPD and 0.38 mg mL^{-1} PVK.

Substrates were 3 × 3 cm soda-lime glass onto which Cr (2 nm bonding layer), Au (100 nm), and molybdenum oxide (MoO_3, Alfa Aesar Puratronic, 99.9995% purity, 10 nm) were evaporated in an Angstrom Engineering EvoVac system at 1 µTorr. Spin-coating the HTL solution at 1000 rpm for 45 s formed a 20 nm thick layer, followed by thermal annealing for 20 min at 150 °C. A 15 s O_2 plasma etch improved wettability for the subsequent perovskite layer (6000 rpm for 35 s; solvent quench after 5 s with toluene (Sigma–Aldrich, anhydrous 99.8%). The active area of the device (17 × 22 mm) was defined by removing the perovskite and HTL layers from the edges of the sample using a solution of 1:7 ratio by volume of DMF to CB solvents applied via a cotton applicator. Samples were subsequently annealed at 70 °C for 5 min. In vacuum were subsequently deposited 40 nm of 2,2′,2″-(1,3,5-benzinetriyl)-tris(1-phenyl-1-H-benzimidazole) (TPBi), a

bilayer of LiF (1.2 nm) and Al (2 nm), and top-electrode Ag:Al alloy (15:1 volumetric ratio) of ≈11–13 nm thickness. Due to the rapid rate of evaporation (9 Å s^{-1}), the top-electrode thickness varies by 1–2 nm batch-to-batch, which simulation and experiment confirm has a major impact on maximum device EQE (see Table S1, Supporting Information). Outcoupling layers were evaporated over the entire active area of the sample.

Device Characterization: Devices were characterized using a home-made goniometer setup that captures *J–V* performance as well as photon emission using a SiGe photodetector and a spectrometer fiber. Angular emission profiles were collected by sampling photocurrent at viewing angles from 0° to 80° in steps of 10° at a fixed azimuthal angle and radius from the pixel center. Due to our pixel shape and size (rectangular, 2.5 mm^2) we assume azimuthal symmetry in our emission profile and sample only the theta dependence. The LED spectrum and the responsivity of the photodiode were used to determine the total photon emission (see section on calculating EQE in Supporting Information).

Simulation Methods: LED optical performances were simulated using the layer thicknesses and complex indices of refraction of the constituent layers to form the basis of a transfer matrix model (TMM) developed from equations outlined by Furno et al.[35,36] in MATLAB. Smooth interfaces without scattering are assumed. Anisotropy is assumed in recombination event emission direction, consistent with Lambertian profile detected in bottom-emitting architectures. Normalized wavelength from an empirical device was used for ratios and wavelengths emitted from the device, and wavelengths from 600 to 850 nm were included in the simulation. After characterizing all data for a particular outcoupling material, a few simulations were compared to the control devices (with no outcoupling material) to characterize the "base device" for a particular run (Table S1, Supporting Information shows the parameters of best fit for each base device). This captures batch-to-batch variations in layer formation before simulating each outcoupling layer, most importantly the top-electrode and perovskite thickness, the latter of which can change in response to the solvent atmosphere during spin-coating. Simulator output includes a (max) EQE for the structure (for a given electrical efficiency), viewing angle profile, spectral power dissipation plot, and spectrum versus viewing angle, among other data. Electrical efficiency was fit by calculating EQE trends over the tested outcoupling thickness range for a range of efficiencies in steps of 5%. Experimentally calculated maximum EQE values were found to roughly match trends of constant electrical efficiency with slight variations.

COMSOL Multiphysics simulations in Figure 1b and Figure S1 (Supporting Information) were calculated using the Wave Optics Module. Uniform dielectric slabs were modeled using the complex indices of refraction of each layer at our peak emission wavelength (765 nm). Layer thicknesses were taken from typical device parameters. An oscillating electric field was placed in the center of the emissive layer. Electric field strengths were plotted on a normalized color scale, showing locations in the microcavity structure where electric fields are stronger. The structure of the cavity affects the mode densities in the LED microcavity which corroborate the peak and trough EQE performances for each of the dielectric outcoupling layers.

Supporting Information

Supporting Information is available from the Wiley Online Library or from the author.

Acknowledgements

The authors acknowledge support for this work from the Eric and Wendy Schmidt Transformative Technology Fund, DARPA under Award No. N66001-20-1-4052, and the National Science Foundation under Award No. ECCS-2222043. The authors would like to acknowledge the contributions of Lianfeng Zhao, William Gunnarsson, and Nakita Noel for experimental advice and troubleshooting during this project.

Conflict of Interest

The authors declare no conflict of interest.

Data Availability Statement

The data that support the findings of this study are available from the corresponding author upon reasonable request.

Keywords

LED, outcoupling, perovskite, simulation, top-emitting

Received: October 6, 2024
Revised: October 9, 2024
Published online: November 13, 2024

[1] Y. Miao, L. Cheng, W. Zou, L. Gu, J. Zhang, Q. Guo, Q. Peng, M. Xu, Y. He, S. Zhang, Y. Cao, R. Li, N. Wang, W. Huang, J. Wang, *Light Sci. Appl.* **2020**, *9*, 89.
[2] L. Zhao, K. Roh, S. Kacmoli, K. A. Kurdi, X. Liu, S. Barlow, S. R. Marder, C. Gmachl, B. P. Rand, *Adv. Mater.* **2021**, *33*, 2104867.
[3] J. Chen, P. Ma, W. Chen, Z. Xiao, *Nano Lett.* **2021**, *21*, 8426.
[4] L. Zhao, K. M. Lee, K. Roh, S. U. Z. Khan, B. P. Rand, *Adv. Mater.* **2019**, *31*, 1805836.
[5] H. Xu, X. Wang, Y. Li, L. Cai, Y. Tan, G. Zhang, Y. Wang, R. Li, D. Liang, T. Song, B. Sun, *J. Phys. Chem. Lett.* **2020**, *11*, 3689.
[6] T. Lee, D. Hahm, K. Kim, W. K. Bae, C. Lee, J. Kwak, *Small* **2019**, *15*, 1905162.
[7] M. Lu, J. Guo, S. Sun, P. Lu, J. Wu, Y. Wang, S. V. Kershaw, W. W. Yu, A. L. Rogach, Y. Zhang, *Nano Lett.* **2020**, *20*, 2829.
[8] L. N. Quan, B. P. Rand, R. H. Friend, S. G. Mhaisalkar, T. W. Lee, E. H. Sargent, *Chem. Rev.* **2019**, *119*, 7444.
[9] L. Zhao, K. Roh, S. Kacmoli, K. AlKurdi, S. Jhulki, S. Barlow, S. R. Marder, C. Gmachl, B. P. Rand, *Adv. Mater.* **2020**, *32*, 2000752.
[10] Z. Chen, R. L. Z. Hoye, H. Yip, N. Fiuza-Maneiro, I. López-Fernández, C. Otero-Martínez, L. Polavarapu, N. Mondal, A. Mirabelli, M. Anaya, S. D. Stranks, H. Liu, G. Shi, Z. Xiao, N. Kim, Y. Kim, B. Shin, J. Shi, M. Liu, Q. Zhang, Z. Fan, J. C. Loy, L. Zhao, B. P. Rand, H. Arfin, S. Saikia, A. Nag, C. Zou, L. Y. Lin, H. Xiang, et al., *J. Phys. Photonics* **2024**, *6*, 032501.
[11] Z. Xu, H. Bristow, M. Babics, B. Vishal, E. Aydin, R. Azmi, E. Ugur, B. Yildirim, J. Liu, R. Kerner, S. De Wolf, B. P. Rand, *Joule* **2023**, *7*, 1992
[12] J. Hong, Z. Xu, D. Lungwitz, J. Scott, H. M. Johnson, Y. Kim, A. Kahn, B. P. Rand, *ACS Energy Lett.* **2023**, *8*, 4984.
[13] P. Schulz, J. O. Tiepelt, J. A. Christians, I. Levine, E. Edri, E. M. Sanehira, G. Hodes, D. Cahen, A. Kahn, *ACS Appl. Mater. Interfaces* **2016**, *8*, 31491.
[14] D. Chen, S. Pang, L. Zhou, X. Li, A. Su, W. Zhu, J. Chang, J. Zhang, C. Zhang, Y. Hao, *J. Mater. Chem. A* **2019**, *7*, 15156.
[15] W. Li, W. Cao, H. Zhou, X. Zhang, K. Wang, *RSC Adv.* **2024**, *14*, 2757.
[16] P. Andričević, G. Náfrádi, M. Kollár, B. Náfrádi, S. Lilley, C. Kinane, P. Frajtag, A. Sienkiewicz, A. Pautz, E. Horváth, L. Forró, *Sci. Rep.* **2021**, *11*, 17159.
[17] W. Xu, F. Li, Z. Cai, Y. Wang, F. Luo, X. Chen, *J. Mater. Chem. C* **2016**, *4*, 9651.
[18] Y. Jia, R. A. Kerner, A. J. Grede, B. P. Rand, N. C. Giebink, *Adv. Opt. Mater.* **2020**, *8*, 1901514.
[19] W. B. Gunnarsson, B. P. Rand, *APL Mater.* **2020**, *8*, 30902.
[20] K. Roh, L. Zhao, B. P. Rand, *ACS Photonics* **2021**, *8*, 2548.
[21] G. Mei, Y. Zhang, B. Xu, *Nanotechnology* **2023**, *34*, 175201.

[22] K. Roh, L. Zhao, W. B. Gunnarsson, Z. Xiao, Y. Jia, N. C. Giebink, B. P. Rand, *ACS Photonics* **2019**, *6*, 3331.
[23] J. Qin, X. K. Liu, C. Yin, F. Gao, *Trends Chem.* **2021**, *3*, 34.
[24] Y. Jia, R. A. Kerner, A. J. Grede, B. P. Rand, N. C. Giebink, *Nat. Photonics* **2017**, *11*, 784.
[25] L. Zhao, D. D. Astridge, W. B. Gunnarsson, Z. Xu, J. Hong, J. Scott, S. Kacmoli, K. A. Kurdi, S. Barlow, S. R. Marder, C. F. Gmachl, A. Sellinger, B. P. Rand, *Nano Lett.* **2023**, *23*, 4785.
[26] M. Yan, L. Zhou, L. Wang, G. Luo, L. Xu, D. Yang, Y. Fang, *Small* **2024**, *20*, 2309233.
[27] G. Mei, X. Xiao, S. Ahmad, H. Lin, Y. Tan, K. Wang, X. W. Sun, W. C. H. Choy, *Adv. Opt. Mater.* **2023**, *11*, 2300912.
[28] W. Qiu, Z. Xiao, K. Roh, N. K. Noel, A. Shapiro, P. Heremans, B. P. Rand, *Adv. Mater.* **2019**, *31*, 1806105.
[29] E. M. Sanehira, B. J. Tremolet De Villers, P. Schulz, M. O. Reese, S. Ferrere, K. Zhu, L. Y. Lin, J. J. Berry, J. M. Luther, *ACS Energy Lett.* **2016**, *1*, 38.
[30] M. T. Greiner, L. Chai, M. G. Helander, W. M. Tang, Z. H. Lu, *Adv. Funct. Mater.* **2013**, *23*, 215.
[31] C. Zhang, N. Kinsey, L. Chen, C. Ji, M. Xu, M. Ferrera, X. Pan, V. M. Shalaev, A. Boltasseva, L. J. Guo, *Adv. Mater.* **2017**, *29*, 1605177.
[32] H. R. Mahida, D. Singh, Y. Sonvane, S. K. Gupta, P. B. Thakor, *Solid State Commun.* **2017**, *252*, 22.
[33] K. Xu, C. Lu, Y. Huang, J. Hu, X. Wang, *RSC Adv.* **2017**, *7*, 54876.
[34] T. Fukushima, H. Kaji, *Org. Electron.* **2012**, *13*, 2985.
[35] M. Furno, R. Meerheim, S. Hofmann, B. Lüssem, K. Leo, *Phys. Rev. B* **2012**, *85*, 115205.
[36] M. Furno, R. Meerheim, M. Thomschke, S. Hofmann, B. Lüssem, K. Leo, in *Light-Emitting Diodes: Materials, Devices, and Applications for Solid State Lighting XIV*, San Francisco, CA, United States, February, **2010**.
[37] L. Zhao, N. Rolston, K. M. Lee, X. Zhao, M. A. Reyes-Martinez, N. L. Tran, Y. W. Yeh, N. Yao, G. D. Scholes, Y. L. Loo, A. Selloni, R. H. Dauskardt, B. P. Rand, *Adv. Funct. Mater.* **2018**, *28*, 1802060.